

Theoretical estimation of optical gain in Tin-incorporated group IV alloy based transistor laser

Ravi Ranjan¹  · Mukul K. Das¹

Received: 2 October 2015 / Accepted: 2 February 2016 / Published online: 19 February 2016
© Springer Science+Business Media New York 2016

Abstract We have calculated the electronic band structure and polarization dependent optical gain in a strain balanced $\text{Si}_x\text{Ge}_y\text{Sn}_{1-x-y}/\text{Ge}_z\text{Sn}_{1-z}$ based transistor laser (TL) with $\text{Ge}_z\text{Sn}_{1-z}$ single quantum well (QW) in the base. Design consideration for QW is also addressed to ensure moderate carrier and optical confinement. A significant TE mode optical gain is obtained in mid infra red region for the transition of Γ valley conduction band to heavy hole valence band. Optical gain in the QW plays an important role in determining the optical characteristics of Tin (Sn) incorporated group IV material based TL.

Keywords Transistor laser · GeSn alloy · Compressive strain · TE polarized gain · Quantum well · Threshold carrier density

1 Introduction

III–V based TL has already proven its performance (Feng et al. 2005, 2007; Holonyak and Feng 2006) but the cost of device is high and so not suitable for commercial use. Group IV semiconductor like Si and Ge are always a good choice of materials for devices particularly for integrated circuit devices because of their low cost and matured growth technology. Yet these materials are not suitable for light emitting devices because of their indirect bandgap nature. However, direct Γ valley of the Ge conduction band is only 134 meV higher than

This article is part of the Topical Collection on Numerical Simulation of Optoelectronic Devices, NUSOD' 15.

Guest edited by Julien Javaloyes, Weida Hu, Slawek Sujecki and Yuh-Renn Wu.

✉ Ravi Ranjan
ranjan275@gmail.com

¹ UGC-SAP Research Laboratory, Department of Electronics Engineering, Indian School of Mines, Dhanbad, India

the indirect L valley. It says that with band-structure engineering, Ge has the potential to become a direct band gap material which can be used for efficient light emitting devices (Kouvetakis et al. 2006). Although several approaches have reported in this context (Goodman 1982; Soref and Perry 1991; Fischetti and Laux 1996; Kurdi et al. 2009), incorporation of Sn into Ge lattice is most promising route to obtain direct band gap in Ge (Kouvetakis et al. 2006).

Some studies on GeSn alloy based optoelectronic devices such as lasers (Chang et al. 2010), detectors (Werner et al. 2011) etc. have already been reported in literature. But, GeSn alloy based TL has not yet been reported to the best of authors knowledge. Moreover, due to large lattice mismatch between Ge and Sn, strain energy builds up and it plays important role on the nature of transition in GeSn alloy. As TL is QW based devices, the study of quantum mechanical behavior of GeSn active layer is also important. Thus, proper design of GeSn based TL considering the design criteria like significant carrier and optical confinement is really a big challenge. To the best of authors knowledge no such design aspects has yet been discussed and reported in literature. Theoretical model for Group-IV based TL to predict Sn composition dependent optical gain have already been proposed by the authors elsewhere (Das and Ranjan 2015). The work has been extended further to study the characteristic of quantum mechanical behavior of the active layer of proposed TL and is reported here. Also, subband carrier distribution is considered for determination of optical gain and threshold carrier density. Rest of the paper is organized as follows. Design aspect and proposed device structure for strain balanced GeSn-based TL is described in Sect. 2. Simulation results are discussed in Sect. 3 and in last section, conclusion is made.

2 Design aspects and proposed model

Band edges of Γ and L valleys in conduction band, heavy hole (HH) and light hole (LH) in valance band are calculated using model solid theory (Van de Walle 1989) where parameters for Si, Ge and Sn are taken from different literatures. Values of relevant material parameters along with the references from where they are taken are summarized in Table 1 for quick reference. Model solid theory uses self-consistent first principle calculation to derive the relative energies of the valance and the conduction band at semiconductor interfaces. In our calculation, interface between two lattice matched surfaces is assumed to be ideal, whereas pseudomorphic potential due to strain in each layer is considered for the interface between two lattice mismatched surfaces. Band edges in Ge and in $\text{Ge}_{0.85}\text{Sn}_{0.15}$ are calculated considering strain and are shown in Fig. 1a, b respectively. It is seen from Fig. 1a that the direct bandgap can be obtained in tensile strained Ge layer at a minimum strain of 1.61 %. Moreover, in the case of tensile strained Ge, LH is higher than HH band and so, the TM polarized gain will be dominating over TE mode gain. But the optical confinement factor, high value of which is required for lasing operation, is poorer in TM mode than that in TE mode (Chuang 2009). Now, it is seen from Fig. 1b that the direct bandgap can also be obtained in compressively strained $\text{Ge}_{0.85}\text{Sn}_{0.15}$ layer and minimum value of required strain is 0.72 % (absolute value) for Sn composition of 15 %. It is also seen from Fig. 1b that in case of compressively strained GeSn, HH is higher than LH band and so, the TE polarized gain will dominate. So, GeSn alloy material is preferred to be the active layer material of a light emitting device. In this context, it may be mentioned that the range of compressive strain, for which GeSn shows direct bandgap nature, varies with Sn concentration in GeSn alloy. This range is 0–72 % for Sn

Table 1 Parameters of Si, Ge, α -Sn (Chang et al. 2010; Van de Walle 1989; Menendez and Kouvetakis 2004)

Parameters	Si	Ge	α -Sn
Lattice constants (\AA)	a 5.4307	5.6573	6.4892
Effective masses (m_0)	m_c 0.528	0.038	0.058
Luttinger's parameter	γ_1 4.22	13.38	-14.97
Average valance band energies (eV)	ΔE_{val} -0.48	0	0.69
Bandgaps (eV)	$E_{\text{g,L}}$ 4.185	0.798	-0.41
Deformation potentials (eV)	a_L -10.06	-8.24	-6.00
	b_v 2.46	1.24	1.58
Elastic constants (GPa)	C_{11} 165.77	128.53	69.00
Refractive index	η 3.434	4.051	5.791
		0.664	0.09
		-1.54	-2.14
		-2.9	-2.7
		48.26	29.30
			0.8

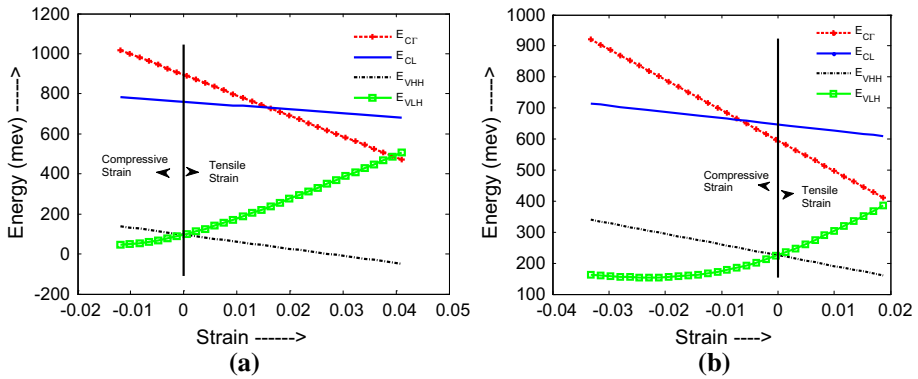


Fig. 1 **a** Band edges of Ge as a function of Strain. Indirect to direct band edge at tensile strain 1.61 %. In tensile strain LH is above then HH. 1. **b** Band edges of $Ge_{0.85}Sn_{0.15}$ as a function of Strain. Indirect to direct band edge at compressive strain 0.72 %. In compressive strain HH is above then LH

concentration of 15 % as shown in Fig. 1b. For larger values of Sn composition, this range will be higher. However, in summary, it can be accomplished that, higher value of absolute strain is required in tensile strained Ge than compressively strained Gesn to achieve direct band gap in Group-IV material. Lower value of strain reduces the misfit dislocation density in strained layer and hence improves the fabrication quality of deposited layer. Now, the barrier region requires higher bandgap and lower refractive index material like Si, Ge etc. to ensure carrier and optical confinement. But the bandgap between direct (Γ valley) and indirect (L valley) is much higher in Si than Ge. Thus, by choosing Si-incorporated alloy, e.g. SiGeSn as a material for barrier serves both the purposes. So, the ternary material SiGeSn is used as a barrier for better optical and carrier confinement. However, with increasing Sn concentration in SiGeSn, energy difference between Γ and L valley in the barrier reduces but refractive index of barrier increases which causes reduced optical confinement. Thus a tradeoff occurs between carrier and optical confinement. So, choice of Sn concentration for both, well and barrier is very important.

The schematic diagram of the proposed TL considered in our model is shown in Fig. 2. The n-type Si material forms an emitter, the p-type $Si_{0.12}Ge_{0.73}Sn_{0.15}$ as a base and n-type

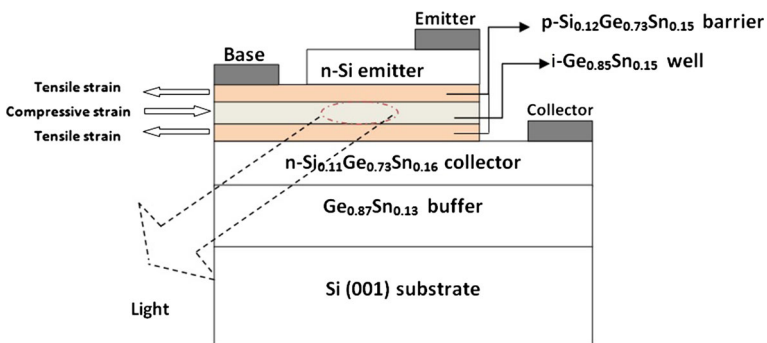


Fig. 2 Schematic structure of *npn* Si - $Si_{0.12}Ge_{0.73}Sn_{0.15}$ - $Si_{0.11}Ge_{0.73}Sn_{0.16}$ based transistor laser (TL) with strain-balanced *i-Ge_{0.85}Sn_{0.15}* single quantum well (QW) in the base. Strain relaxed $Ge_{0.87}Sn_{0.13}$ buffer layer is used to create compressive strain in well and tensile strain in barrier

Si_{0.11}Ge_{0.73}Sn_{0.16} as a collector. For lasing action, an intrinsic Ge_{0.85}Sn_{0.15} QW is inserted in the Si_{0.12}Ge_{0.73}Sn_{0.15} base which acts as a barrier. The collector layer is lattice matched with strain-relaxed Ge_{0.87}Sn_{0.13} buffer layer which is used for subsequent growth of barrier and well. The composition of buffer is chosen such that the strains observed by well and barrier are equal but opposite in nature. Thus, 0.18 % of tensile strain in barrier compensates 0.29 % compressive strain in the well. The well width is selected such that single bound state exists in each of conduction band and valence band. Also, width of the well is chosen by taking critical thickness of GeSn layer into consideration. Barrier width of 80 Å is calculated for 100 Å thick well using strain balanced condition for a cubic based multilayer system grown along (001) axis (Van de Walle 1989). The growth of such strained layer Ge_zSn_{1-z} is demonstrated experimentally (Oehme et al. 2014).

3 Theoretical calculation and results

The bandgaps of unstrained GeSn and SiGeSn material system are calculated from the expression given by (Chang et al. 2010):

$$\begin{aligned}
 E_{g\eta_SiGeSn} &= xE_{g\eta_Si} + yE_{g\eta_Ge} + (1 - x - y)E_{g\eta_Sn} - xyb_{\eta_SiGe} \\
 &\quad - x(1 - x - y)b_{\eta_SiSn} - y(1 - x - y)b_{\eta_GeSn} \tag{1} \\
 E_{g\eta_GeSn} &= zE_{g\eta_Ge} + (1 - z)E_{g\eta_Sn} - z(1 - z)b_{\eta_GeSn}
 \end{aligned}$$

where η stands for Γ and L valley. Bowing parameters, b_{η_SiGe} , b_{η_SiSn} and b_{η_GeSn} of SiGe, SiSn and GeSn are listed in Table 2 (Chang et al. 2010). Linear interpolation technique is used to obtain other material parameters of Ge_zSn_{1-z} and Si_xGe_ySn_{1-x-y}. In the model solid theory, average of three valance band (VB) at Γ valley are taken as a reference level so all the band edges are calculated at Γ point of the Brillouin zone. Due to deformation potential and spin orbit effect the valance band shifted from average valance band. The VB energy of unstrained Ge_zSn_{1-z} given by:

$$E_{v_GeSn} = E_{v_avg_GeSn} + \frac{1}{3}\Delta_{0_GeSn} \tag{2}$$

where, $E_{v_avg_GeSn}$ and Δ_{0_GeSn} is average valance band and spin orbit splitting energy of GeSn respectively.

The conduction band (CB) of unstrained GeSn is calculated using:

$$E_{c\eta_GeSn} = E_{v_GeSn} + E_{g\eta_GeSn} \tag{3}$$

Since our growth direction along (001) axis, strain along the surface (x, y) is same. The CB for strained Ge_zSn_{1-z} given by:

$$E_{c\eta_GeSn_strain} = E_{c\eta_GeSn} + a_{c\eta_GeSn}(e_{xx_GeSn} + e_{yy_GeSn} + e_{zz_GeSn}) \tag{4}$$

Table 2 Bowing parameter of SiGe, GeSn, SiSn (Chang et al. 2010)

Bowing parameter		SiGe		GeSn		SiSn	
b _L (eV)	b _Γ (eV)	0.169	0.21	1.23	1.94	0.925	13.2

where, $a_{c\eta_GeSn}$ is hydrostatic deformation potential for CB. e_{xx_GeSn} , e_{yy_GeSn} and e_{zz_GeSn} are strain along x, y and z axis respectively. Due to shear strain, VB splits into HH and LH band. The expression of HH and LH valance band given by:

$$\begin{aligned}
 E_{v_HH_GeSn} &= E_{v_avg_GeSn} + a_{v_GeSn}(e_{xx_GeSn} + e_{yy_GeSn} + e_{zz_GeSn}) + \frac{1}{3}\Delta_{0_GeSn} - \frac{1}{2}\delta E_{_GeSn} \\
 E_{v_LH_GeSn} &= E_{v_avg_GeSn} + a_{v_GeSn}(e_{xx_GeSn} + e_{yy_GeSn} + e_{zz_GeSn}) \\
 &\quad - \frac{1}{6}\Delta_{0_GeSn} + \frac{1}{4}\delta E_{_GeSn} + \frac{1}{2}\left[\Delta_{0_GeSn}^2 + \Delta_{0_GeSn}\delta E_{_GeSn} + \frac{9}{4}\delta E_{_GeSn}^2\right]^{1/2}
 \end{aligned}
 \tag{5}$$

where change in energy due to shear strain is

$$\delta E_{_GeSn} = 2b_{v_gesn}(e_{zz_GeSn} - e_{xx_GeSn})
 \tag{6}$$

The band offsets between the well and the barrier in Γ -CB and HH, LH valance band are as follows:

$$\begin{aligned}
 \Delta E_{C\Gamma} &= E_{C\Gamma_SiGeSn_strain} - E_{C\Gamma_GeSn_strain} \\
 \Delta E_{V_HH} &= E_{V_HH_GeSn} - E_{V_HH_SiGeSn} \text{ and } \Delta E_{V_LH} = E_{V_LH_GeSn} - E_{V_LH_SiGeSn}
 \end{aligned}
 \tag{7}$$

where av_GeSn is deformation potential of VB and $bc\eta_GeSn$ is deformation potential for shear strain.

The band offsets of $Si_{0.12}Ge_{0.73}Sn_{0.15}$ barrier and $Ge_{0.85}Sn_{0.15}$ well are used to find Eigen energies and corresponding wave functions in Γ -CB, HH and LH VB. In Γ -conduction band, following Schrödinger equation with effective mass approximation is used to obtain the Eigen energy and the wave function (Chuang 2009):

$$\left[\frac{-\hbar^2}{2} \frac{\partial}{\partial z} \frac{1}{m_C} \frac{\partial}{\partial z} + \frac{\hbar^2 k_t^2}{2m_C} + V_C(z) \right] \psi = E_C \psi
 \tag{8}$$

where z is position variable, ψ is wave function. E_C , m_c are Eigen energy and effective mass in Γ -CB respectively. k_t is wave vector perpendicular to k_z (growth axis) and directed along $\langle 110 \rangle$ in k_x-k_y plane. V_C is the potential profile of Γ -CB which includes strain effect. In the above Schrödinger equation ψ does not contain the Bloch function because effect of periodic potential created by crystal lattice is replaced by effective mass m_c . To reduce the complexity of problem, all calculation are around Γ point of the Brillouin zone thus, we take $k_t = 0$. The Schrödinger equation is solved using one of the numerical techniques, Finite Difference Method (FDM) (Datta 2005). The lowest Eigen energy value is 1st subband energy in Γ CB and its corresponding Eigen vector is wave function. The VB is degenerate in energy so interaction between the bands cannot be neglected. The effect of HH band on LH band and vice versa are shown by an extra coupling term in the Schrödinger equation (Coldren et al. 2012). Due to strain effect HH and LH band are split and it is assume that if difference between band edge of HH and LH at Γ point ($k_t = 0$) is large enough then the coupling between HH and LH can be neglected (Coldren et al. 2012). With this assumption we take Schrödinger equation for HH and LH valance band as follows (Chuang 2009):

$$\left[\frac{-\hbar^2}{2} \frac{\partial}{\partial z} \frac{1}{m_{V_hh, lh}} \frac{\partial}{\partial z} + \frac{\hbar^2 k_t^2}{2m_{V_hh, lh}} + V_{hh, lh}(z) \right] \psi = E_{V_hh, lh} \psi \tag{9}$$

where $m_{V_hh} = \frac{m_0}{\gamma_1 - 2\gamma_2}$ and $m_{V_lh} = \frac{m_0}{\gamma_1 + 2\gamma_2}$ uses to replace the effect of Bloch function. f_+ is dimensionless strain dependent factor which comes from spin orbit effect.

Calculated band alignment, Eigen energies and wave function for well and barrier in base are shown in Fig. 3a and band diagram at equilibrium for the region of emitter to collector of the device considering Γ -valley CB and HH VB is shown in Fig. 3b. In Fig. 3a, band offset between the well and the barrier is finite thus wave function is not confined only in the well region. However, it is sufficiently large to ensure carrier confinement in the well. Compressive strain is present in the well so, HH valance band is above the LH valance band but it is reverse in barrier region. It is also observed that the band edges of L valley in the well and the barrier are higher than the band edge of Γ -valley in the well and thus, the direct bandgap is obtained in the well. It is clear from the figure that a single quantized level in Γ -conduction band, HH band and LH band is present for the said dimension of well.

Optical gain is an important parameter for analysis of laser performance and it estimated for the strain-balanced QW structure with the help of Fermi golden rule (Chuang 2009). Eigen energies and wave function are taken along z-direction in the conduction band and HH band. The expression for gain coefficient is given by:

$$g(\hbar\omega) = C_0 |I_{hh}^1|^2 \int_0^\infty dE_t \rho_r^{2D} |\hat{e} \cdot p_{cv}|^2 \frac{H/2\pi}{[E_{hh}^1(0) + E_t - \hbar\omega]^2 + (H/2)^2} [f_c^1(\hbar\omega) - f_v^1(\hbar\omega)] \tag{10}$$

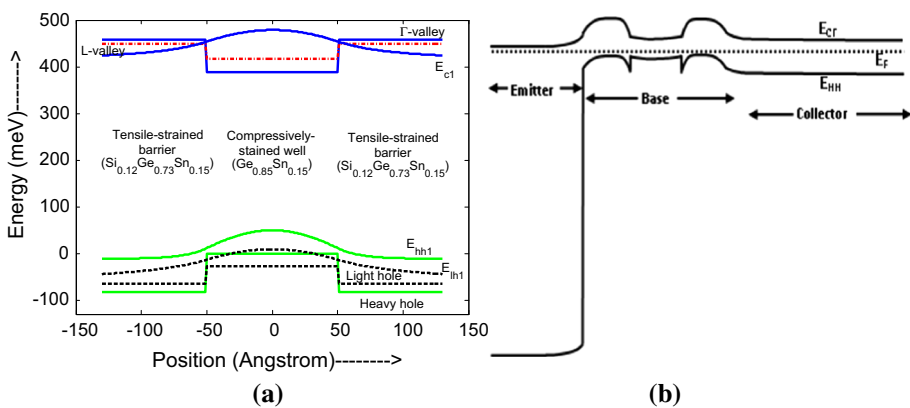


Fig. 3 **a** The Energy band structure, Eigen energy and wave function for $Ge_{0.85}Sn_{0.15}/Si_{0.12}Ge_{0.73}Sn_{0.15}$ QW is shown in figure. In well, compressive strain is present so HH valance band is above then LH valance band and reverse in barrier region. **b** Band structure of the device (from emitter to collector) at equilibrium considering Γ -valley conduction band and HH valance band

where

$$C_0 = \frac{\pi e^2}{n_r c \epsilon_0 m_0^2 w}, \rho_r^{2D} = \frac{m_r}{\pi \hbar^2 L_z}, I_{h1}^{e1} = \sum_{-L_z/2}^{L_z/2} \phi_1(z) g_1(z), \quad (11)$$

$$|\hat{e} \cdot p_{cv}|^2 = 1.5 \left(\frac{m_0}{m_e} - 1 \right) \frac{m_0 E_g (E_g + \Delta)}{6(E_g + \frac{2}{3}\Delta)}$$

where n_r is refractive index of GeSn, ρ_r^{2D} is reduced density of state function, L_z is width of QW along z-direction, and m_r is reduced effective mass. I is overlap integral of the conduction subband wave function ($\Phi_1(z)$) and valance subband wave function ($g_1(z)$). $|\hat{e} \cdot p_{cv}|^2$ is momentum matrix element between the CB and the VB, where \hat{e} is polarization unit vector. H is the full-width at half-maximum (FWHM) of the Lorentzian function, which is taken as 20 meV (Chang et al. 2010). E_{h1}^{e1} is the bandgap between E_{c1} and E_{h1} which are bound state Eigen energies in Γ conduction band and HH valance band respectively. The Fermi occupation probabilities (f_c^n and f_v^m) are expressed as follows:

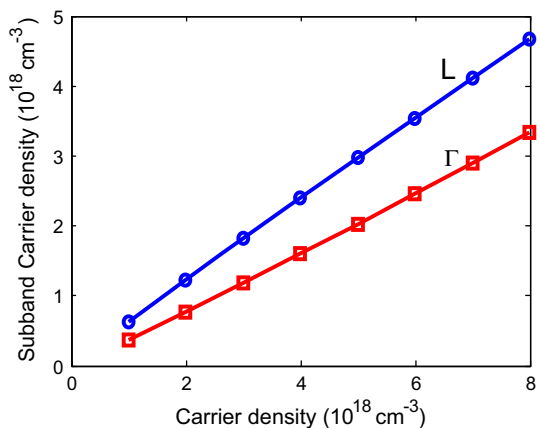
$$f_c^n(\hbar\omega) = \frac{1}{1 + \exp\{[E_{C1} + (m_r/m_e)(\hbar\omega - E_g) - F_c]/K_B T\}}, \quad (12)$$

$$f_v^m(\hbar\omega) = \frac{1}{1 + \exp\{[E_{h1} - (m_r/m_h)(\hbar\omega - E_g) - F_v]/K_B T\}}$$

here the F_c and F_v are the quasi-Fermi level which are calculated for a given injected carrier density (Chuang 2009). We considered charge neutrality condition and neglected the effect of p-type barrier because our model has intrinsic QW.

In the proposed structure injected carriers reach to the well through the barrier. Carrier density distribution in Γ conduction valley and L conduction valley is required to predict more accurate value of optical gain. The carrier density in different subbands with total injected carrier density in the well is shown in Fig. 4. In the barrier region L conduction valley has lower potential compared to Γ conduction valley so large amount of carrier goes to L valley in the barrier region that further transport to L valley in the well. However the difference in L and Γ conduction valley in the barrier region is very less so a significant amount of carrier goes to Γ conduction valley in the well. Although the current injection

Fig. 4 Carrier densities of Γ and L conduction valley as a function of total injected carrier density



efficiency is poor, the significant amount of carriers in gamma valley in the well will recombine radiatively which is sufficient for lasing action. We can increase the gain by heavily doped emitter or by changing Sn concentration in well and barrier. So GeSn QW has the potential to provide gain medium for optoelectronic applications. Benefits of GeSn quantum well are its ease of integrability by matured CMOS technology and its toxicity. In Fig. 5, optical gain for different total injected carrier densities is plotted as a function of photon energy. Out of total injected carrier, the leakage carrier density in L valley does not contribute to the optical gain. It is clear from figure that, with increase in injected carrier density, the optical gain increases, as the difference in fermi occupation probabilities increases. The spectral width also increases with increasing injected carrier density ($E_{cl}^{h1} > hv > F_{CV}$) as shown in Fig. 5. As injected carrier density increases, quasi-fermi level separation ($F_{CV} = F_C - F_V$) also increases. Hence, the range of positive gain ($E_{cl}^{h1} > hv > F_{CV}$) is increased. The peak TE gain is obtained at 460 meV, corresponding to a emission wavelength of 2.68 μm , which lies in mid-infrared region. To predict the transparency carrier density and the threshold carrier density, the modal gain and the threshold modal gain are plotted as a function of total injected carrier density and are shown in Fig. 6. It is observed from figure that modal gain increases with total injected carrier density and reaches to the threshold value for the carrier density of $4.9 \times 10^{18} \text{ cm}^{-3}$ which is nothing but threshold carrier density (N_{th}). Modal gain crosses the zero value at carrier density of $2.1 \times 10^{18} \text{ cm}^{-3}$ which is the transparency carrier density, N_{tr} . In this calculation, optical confinement factor is taken as 5 %, the cavity length is taken as 500 μm , the reflectivities (R_1 & R_2) for both the facets of the cavity are taken as 0.357 and modal loss is taken from (Chang et al., 2010). The differential gain g is obtained as $4.32 \times 10^{-17} \text{ cm}^2$.

One of the important parameters, DC current gain of the transistor can be obtained from base current and collector current calculation which again need solution of continuity and rate equations in the base. An estimation of current gain is obtained and it is approximately in the range of 100–120 for the doping in the barrier $\sim 10^{19} \text{ cm}^{-3}$. Also, it is found that, with increasing base current, the dc current gain remains constant initially and after the base threshold current it decreases. This is due to the fact that, above the base threshold current, lasing action starts and due to the significant recombination of carriers in the base, collector current and, hence, current gain decreases. Further study is required for dc and ac analysis of the transistor in detail.

Fig. 5 TE mode gain spectra for different total injected carrier densities. The peak TE gain is obtained at 460 meV, corresponding to a emission wavelength of 2.68 μm , which is in mid-infrared region

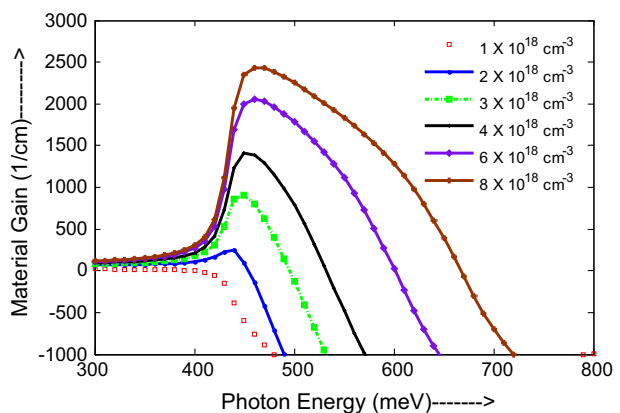


Fig. 6 The Modal gain and threshold modal gain as a function of total injected carrier density



4 Conclusion

In the present work we proposed an analytical model for Tin incorporated n-p-n TL. The effect of concentration of α -Sn and strain in well and barrier regions on optical and carrier confinement, is studied. The $\text{Ge}_z\text{Sn}_{1-z}$ well is chosen to be compressive strained as it supports TE mode which is crucial for higher optical confinement. Ternary material $\text{Si}_x\text{Ge}_y\text{Sn}_{1-x-y}$ add more flexibility in barrier region to control carrier distribution in L and Γ valley. The effect of subband carrier distribution in L valley and Γ valley was also considered in our analysis. The calculated optical gain is used to find transparency carrier density, $N_{\text{tr}} = 2.2 \times 10^{18} \text{ cm}^{-3}$, threshold carrier density, $N_{\text{th}} = 4.9 \times 10^{18} \text{ cm}^{-3}$ and differential optical gain $g = 4.32 \times 10^{-17} \text{ cm}^2$. The peak value of optical gain occurs at $2.68 \mu\text{m}$. So, this device is a potential candidate for low cost monolithic TL for infrared applications. Now, as the barrier height is very less in the proposed structure for TL, effect of temperature on the performance of the device is significant. Rate of escape (inverse of escape lifetime) of carriers, from the well, increases significantly with temperature where as the rate carrier capture in the well varies insignificantly with temperature. Since, the ratio of escape rate to the capture rate has important role on the laser gain, low temperature of operation is always preferred for such devices.

Acknowledgments This work is partly supported by UGC, Govt. of India through the SAP Project Grant for the Department of Electronics Engineering in the thrust area, Modeling of Semiconductor Nanostructured Devices.

References

- Chang, G.E., Chang, S.W., Chuang, S.L.: Strain-balanced multiple-quantum-well lasers. *IEEE J. Quantum Electron.* **46**(12), 1813–1820 (2010)
- Chuang, S.L.: *Physics of photonic devices*, 2nd edn. Wiley, New York (2009)
- Coldren, L.A., Corzine, S.W., Mashanovitch, M.L.: *Diode laser and photonic integrated circuits*, 2nd edn. Wiley, New York (2012)
- Das, M.K., Ranjan, R.: Theoretical estimation of optical gain in Tin-incorporated group IV transistor laser. *Proc. of Int. Conf. NUSOD Post-Deadline Paper*, 9–10 (2015)
- Datta, S.: *Quantum transport: atom to transistor*. Cambridge University Press, New York (2005)
- Goodman, C.H.L.: Direct-gap group IV semiconductors based on tin. *IEEE Proc. I: Solid State Electron Devices* **129**, 189–192 (1982)

- Feng, M., Holonyak Jr, N., Walter, G., Chan, R.: Room temperature continuous wave operation of a heterojunction bipolar transistor laser. *Appl. Phys. Lett.* **87**, 131103 (2005)
- Feng, M., Holonyak Jr, N., Then, H.W., Walter, G.: Charge control analysis of transistor laser operation. *Appl. Phys. Lett.* **91**, 053501 (2007)
- Fischetti, M.V., Laux, S.E.: Band structure, deformation potentials, and carrier mobility in strained Si, Ge, and SiGe alloys. *J. Appl. Phys.* **80**, 2234–2252 (1996)
- Holonyak Jr, N., Feng, M.: The transistor laser. *IEEE Spectr.* **43**, 50–55 (2006)
- Kouvetakis, J., Menendez, J., Chizmeshya, A.V.G.: Tin-based group IV semiconductors: new platforms for opto- and microelectronics on silicon. *Annu. Rev. Mater. Res.* **36**, 497–554 (2006)
- Kurdi, M., El, T., Kociniewski, T.-P., Ngo, J., Boulmer, D., Débarre, D., Boucaud, P., et al.: Enhanced photoluminescence of heavily n-doped germanium. *Appl. Phys. Lett.* **94**, 191107 (2009)
- Menendez, J., Kouvetakis, J.: Type-I Ge/Ge_{1-x-y}Si_xSn_y strained-layer heterostructures with a direct Ge Bandga. *Appl. Phys. Lett.* **85**(7), 1175–1177 (2004)
- Oehme, M., Kostecki, K., Schmid, M., Oliveria, F., Kasper, E., Schulze, J.: Epitaxial growth of strained and unstrained GeSn alloys up to 25 % Sn. *Thin Solid Films* **557**, 169–172 (2014)
- Soref, R.A., Perry, C.H.: Predicted band gap of the new semiconductor SiGeSn. *J. Appl. Phys.* **69**, 539–541 (1991)
- Van de Walle, C.G.: Band lineups and deformation potentials in the model-solid theory. *Phys. Rev. B* **39**(3), 1871–1883 (1989)
- Werner, J., Oehme, M., Schmid, M., Kaschel, M., Schirmer, A., Kasper, E., Schulze, J.: Germanium-tin pin photodetectors integrated on silicon grown by molecular beam epitaxy. *Appl. Phys. Lett.* **98**, 061108 (2011)